This is a preprint, the final version is subject to change, of the American Mineralogist (MSA)
Cite as Authors (Year) Title. American Mineralogist, in press.
(DOI will not work until issue is live.) DOI: http://dx.doi.org/10.2138/am-2016-5508

Revision 3

Crystal chemistry of spinels in the system $MgAl_2O_4$-MgV_2O_4-Mg_2VO_4

FERDINANDO BOSI[1,2*], HENRIK SKOGBY[3], ROSA ANNA FREGOLA[4] AND ULF HÅLENIUS[3]

[1]Dipartimento di Scienze della Terra, Sapienza Università di Roma, Piazzale Aldo Moro 5, I-00185 Roma, Italy
[2]CNR-Istituto di Geoscienze e Georisorse, UOS Roma, Piazzale Aldo Moro 5, 00185 Roma, Italy
[3]Department of Geosciences, Swedish Museum of Natural History, SE-10405 Stockholm, Sweden
[4]Dipartimento di Scienze della Terra e Geoambientali, Università di Bari Aldo Moro, via E. Orabona 4, I-70125 Bari, Italy

ABSTRACT

Eight spinel single-crystal samples belonging to the spinel *sensu stricto*-magnesiocoulsonite series ($MgAl_2O_4$-MgV_2O_4) were synthesized and crystal-chemically characterized by X-ray diffraction, electron microprobe and optical absorption spectroscopy. Site populations show that the tetrahedrally coordinated site (T) is populated by Mg and minor Al for the spinel *sensu stricto* compositions, and only by Mg for the magnesiocoulsonite compositions, while the octahedrally coordinated site (M) is populated by Al, V^{3+}, minor Mg and very minor amounts of V^{4+}. The latter occurs in appreciable amounts in the Al-free magnesium vanadate spinel, $^{T}(Mg)^{M}(Mg_{0.26}V^{3+}_{1.48}V^{4+}_{0.26})O_4$, showing the presence of the inverse spinel VMg_2O_4. The studied samples are characterized by substitution of Al^{3+} for V^{3+} and (Mg^{2+} + V^{4+}) for $2V^{3+}$ described in the system $MgAl_2O_4$-MgV_2O_4-VMg_2O_4.

The present data in conjunction with data from the literature provide a basis for quantitative analyses of two solid solution series $MgAl_2O_4$-$MgV^{3+}_2O_4$ and $MgV^{3+}_2O_4$-$V^{4+}Mg_2O_4$. Unit-cell parameter increases with increasing V^{3+} along the series $MgAl_2O_4$-MgV_2O_4 (8.085-8.432 Å), but only slightly increases with increasing V^{3+} along the series

VMg_2O_4-MgV_2O_4 (8.386-8.432 Å). Although a solid solution could be expected between the $MgAl_2O_4$ and VMg_2O_4 end members, no evidence was found. Amounts of V^{4+} are nearly insignificant in all synthetic Al-bearing vanadate spinels, but are appreciable in Al-free vanadate spinel.

An interesting observation of the present study is that despite the observed complete solid-solution along the $MgAl_2O_4$-MgV_2O_4 and MgV_2O_4-VMg_2O_4 series, the spinel structure seems to be unable to stabilize V^{4+} in any intermediate members on the $MgAl_2O_4$-Mg_2VO_4 join even at high oxygen fugacities. This behavior indicates that the accommodation of specific V-valences can be strongly influenced by crystal-structural constraints, and any evaluation of oxygen fugacities during mineral formation based exclusively on V cation valence distributions in spinel should be treated with caution. The present study underline that the V valency distribution in spinels is not exclusively reflecting oxygen fugacities, but also depends on activities and solubilities of all chemical components in the crystallization environment.

Key-words: Vanadate spinel; magnesiocoulsonite; electron microprobe; crystal synthesis; X-ray diffraction; optical absorption spectroscopy.

INTRODUCTION

Several substances crystallize in the spinel type structure, most of which are multiple oxides. These latter may be defined by the general formula AB_2O_4, where A and B are usually divalent, trivalent and tetravalent cations in the so-called 2-3 spinels ($A^{2+}B^{3+}{}_2O_4$) and 4-2 spinels ($A^{4+}B^{2+}{}_2O_4$). The spinel structure is usually described in the space group $Fd\bar{3}m$ as a slightly distorted cubic close packed array of oxygen anions, in which the A and B cations are distributed in one-eighth of all tetrahedrally-coordinated sites (T) and half of all octahedrally-coordinated sites (M). The unit-cell parameters (*a*, *a*, *a*) and oxygen fractional coordinates (*u*, *u*, *u*) define the resulting tetrahedral (T-O) and octahedral (M-O) bond lengths. The distribution of A and B cations over T and M leads to two different ordered site populations in the 2-3 spinels: (1) normal spinel, where the A^{2+} cation occupies T and the two B^{3+} cations occupy M (e.g., $MgAl_2O_4$, spinel *sensu stricto*); (2) inverse spinel, where one of the B^{3+}

cations occupies T and the remaining A^{2+} and B^{3+} cations occupy M (e.g., $FeFe_2O_4$, magnetite). Similarly, two different types of site populations occur in the 4-2 spinels: (1) normal spinels, in which an A^{4+} cation occupies the T site and two B^{2+} cations occupy the M site (e.g., γ-$SiMg_2O_4$, ringwoodite); (2) inverse spinels, in which a B^{2+} cation occupies T, and the remaining A^{4+} and B^{2+} cations occupy M (e.g., $TiFe_2O_4$, ulvöspinel). Vanadium-bearing spinels are very important in materials science for their electric and magnetic properties (e.g., Miyoshi et al. 2000; Liu et al. 2001) as well as in geosciences for their occurrence in a wide range of geological environments on Earth, Moon, Mars and in meteorites (e.g., Papike et al. 2005; Righter et al. 2006a). Furthermore, their crystal chemistry has been shown to be sensitive to variations in temperature and oxygen fugacity (f_{O2}) conditions (e.g., Canil 1999; Connolly and Burnett 2003; Sutton et al. 2005). Although V may occur in several valence states (from 2+ to 5+), V^{3+} and V^{4+} are the most frequent in the spinel structure (e.g., Papike et al. 2005; Righter et al. 2006a). Natural normal 2-3 spinels may incorporate a significant amount of vanadium into the M site such as in V-bearing magnesiochromite samples ($MgCr_{2-x}V^{3+}_xO_4$) from Sludyanka metamorphic complex in Russia, magnesiocoulsonite ($MgV^{3+}_2O_4$), coulsonite ($Fe^{2+}V^{3+}_2O_4$), and vuorelainenite ($Mn^{2+}V^{3+}_2O_4$) (Radtke 1962; Zakrzewski et al. 1982; Reznitskii et al. 1995; Lavina et al. 2003).

Systematic investigations of the detailed structural variations along the entire series $MgAl_2O_4$-$MgV^{3+}_2O_4$ and $MgV^{3+}_2O_4$-$V^{4+}Mg_2O_4$ are missing in literature. In the present study, we have synthesized spinel single crystals with different compositions along the join $MgAl_2O_4$-MgV_2O_4, and structurally and chemically characterized them by X-ray diffraction, scanning electron microscopy (SEM), electron microprobe (EMP), and optical absorption spectroscopy (OAS). These data are interpreted together with available literature data for compositions along the $MgV^{3+}_2O_4$-$V^{4+}Mg_2O_4$ series to reveal structural details and improve the understanding of factors that affect the crystal chemistry of V-bearing spinels.

EXPERIMENTAL METHODS

Crystal synthesis

Spinel crystals along the $MgAl_2O_4$-MgV_2O_4 join were synthesized from six different starting compositions using a flux-growth method. The spinel components were added as analytical grade oxides which were dried before weighing and then mixed with $Na_2B_4O_7$ used

as the flux component. As the starting composition of the MgV_2O_4 end member contained a large proportion of V_2O_5, which has a low melting point (690 °C), no flux component was added to this run. The charges (ca. 4-5 g) were mixed and ground under acetone in an agate mortar and loaded in 12-ml yttria-stabilized Pt/Au-crucibles which were covered by lids. The crucibles were positioned in the center of a vertical gas-flow tube furnace, and a gas mixture of H_2 and CO_2 with the volume ratio 2:80, corresponding approximately to the Ni-NiO solid buffer, was passed through the furnace tube. Crystal syntheses were carried out as slow-cooling experiments. The temperature was initially raised to 1200°C which was maintained for 24 h to allow melt homogenization, followed by slow cooling (4°C/h) down to 800 °C, from where faster cooling was attained by switching off the furnace elements. In addition to these synthesis experiments performed under reducing conditions, a number of experiments along the $MgAl_2O_4$-MgV_2O_4 and $MgAl_2O_4$-VMg_2O_4 joins were also performed in air using a muffle furnace. Successful runs resulted in octahedral-shaped spinel crystals with sizes ranging from 50 μm to 1 mm embedded in borate-rich glass together with Mg-borates (warwickite) and occasionally V-oxide (karelianite). The borate glass and some of the additional phases were dissolved in dilute HCl and HNO_3 solutions. The color of the spinel crystals synthesized under reducing conditions shifts from orange-red for V-poor samples via dark-red to black for samples progressively richer in vanadium. The spinel crystals synthesized in air, however, were always colorless. As these samples showed cell parameters (based on powder XRD data) indistinguishable from the $MgAl_2O_4$ end member and Energy Dispersive X-ray Spectroscopy analyses of several crystals were unable to detect any vanadium, they were not further studied. Details on the experimental conditions and products of the synthesis runs under reducing conditions are reported in Table 1.

Single-crystal structural refinement

X-ray diffraction measurements were performed at the Earth Sciences Department, Sapienza University of Rome, with a Bruker KAPPA APEX-II single-crystal diffractometer, equipped with a CCD area detector (6.2 × 6.2 cm^2 active detection area, 512 × 512 pixels) and a graphite crystal monochromator, using MoKα radiation from a fine-focus sealed X-ray tube. The sample-to-detector distance was 4 cm. A total of 5088 exposures per sample (step = 0.2°, time/step = 10 s) covering the full reciprocal sphere with a redundancy of about 18 were collected. The orientation of the crystal lattice was determined from 500 to 1000 strong

reflections ($I > 100\ \sigma_I$) evenly distributed in the reciprocal space, and used for subsequent integration of all recorded intensities. Final unit-cell parameters were refined by using the Bruker AXS SAINT program from more than 2000 recorded reflections with $I > 10\ \sigma_I$ in the range $8° < 2\theta < 90°$. The intensity data were processed and corrected for Lorentz, polarization and background effects with the APEX2 software program of Bruker AXS. The data were corrected for absorption using multi-scan method (SADABS). The absorption correction led to a significant improvement in R_{int}. No violation of $Fd\bar{3}m$ symmetry was noted.

Structural refinements were carried out with the SHELXL-2013 program (Sheldrick 2013). Setting the origin at $\bar{3}m$, initial atomic positions for oxygen atoms were taken from the spinel structure (Bosi et al. 2010). Variable parameters were overall scale factor, extinction coefficient, atomic coordinates, site scattering values expressed as mean atomic number (m.a.n.), and atomic displacement factors. No chemical constraint was applied during the refinement. In detail, the T site was modeled with Mg scattering factor, whereas the M site with V and/or Al or Mg scattering factors in accordance with the sample compositions. Three full-matrix refinement cycles with isotropic displacement parameters for all atoms were followed by anisotropic cycles until convergence was attained, that is, when the shifts for all refined parameters were less than their estimated standard deviation. No correlation over 0.7 between parameters or large differences between observed structure factors, such as that of the 222 reflection (e.g., Della Giusta et al. 1986), and the calculated ones were observed at the end of refinement. Table 2 summarizes structural parameters and refinement details, and the corresponding CIFs have been deposited.

Electron microprobe analysis

The same crystals as used for X-ray data collection were mounted on a glass slide and polished for electron microprobe analysis on a Cameca SX50 instrument operated at an accelerating potential of 15 kV and a sample current of 15 nA, with an incident beam diameter of ca. 1 μm. No less than 10 spot analyses for each sample were performed to obtain the average chemical compositions and to estimate compositional homogeneity. Synthetic standards used were MgO (Mg), Al_2O_3 (Al) and V_2O_3 (V). For raw data reduction, the PAP computer program was applied (Pouchou and Pichoir 1984). Spinel formulae were calculated on the basis of 4 oxygen atoms and 3 cations per formula unit (Table 3).

Optical absorption spectroscopy

Unpolarized, optical absorption spectra at 293 K were recorded in the spectral range 33333-10000 cm^{-1} (300-1000 nm) on doubly-sided polished crystal platelets of spinel samples MgV20c and MgV60b. The platelet thicknesses were 10 and 16 μm, respectively. Attempts to prepare absorbers of crystals containing higher V-contents sufficiently thin for recording spectra in the near-UV region were unsuccessful. Even 8 μm thin absorbers of such crystals were opaque above ca. 20000 cm^{-1} (below 500 nm). The recorded spectra of the low-V spinels were obtained at a spectral resolution of 1 nm using an AvaSpec-ULS2048X16 spectrometer (270-1060 nm) attached via a 400 μm UV optical fiber to a Zeiss Axiotron UV-microscope. A 75 W Xenon arc lamp (270-1060 nm) served as illuminating source and Zeiss Ultrafluar 10× lenses served as objective and condenser. The size of the circular measure aperture was 70 μm in diameter. The wavelength scale of the spectrometer was calibrated against Ho_2O_3-doped and Pr_2O_3/Nd_2O_3-doped standards (Hellma glass filters 666F1 and 666F7) with an accuracy better than 15 cm^{-1} in the wavelength range 300-1000 nm.

Cation distribution

The intracrystalline cation distribution was obtained by an optimization program applying a minimization function in which both structural and chemical data (such as bond lengths and site-scattering in terms of equivalent electrons, i.e., mean atomic number) are taken into account. The minimization procedure has been presented and discussed previously (e.g., Carbonin et al. 1996; Lavina et al. 2002; Bosi et al. 2004). Octahedral and tetrahedral bond lengths (M-O and T-O, respectively) were calculated as the linear contribution of each cation multiplied by its specific bond length. The latter are the same used by Uchida et al. (2007) which were based on the studies of Shannon (1976) and Lavina et al. (2002, 2003): ^{T}Mg-O = 1.971 Å, ^{M}Mg-O = 2.082 Å, ^{T}Al-O = 1.774 Å, ^{M}Al-O = 1.908 Å, $^{M}V^{3+}$-O = 2.022 Å and $^{M}V^{4+}$-O = 1.96 Å. Due to crystal-field stabilization energy, a marked octahedrally coordinated site preference is expected for V^{3+} and V^{4+}, thus they were fixed at the M site during the minimization procedure. This assignment is further supported by the spectroscopic measurements. The results are reported in Table 4.

RESULTS AND DISCUSSION

The studied samples belong to the spinel *sensu stricto*-magnesiocoulsonite series, $MgAl_2O_4$-MgV_2O_4. Although most analyzed crystals appear chemically homogeneous, substantial chemical differences were observed between crystals from the same runs. The end-member composition MgV_2O_4 was approached to 95% (crystals MgV90c33 and MgV90c32). The experiment aimed to synthesize the MgV_2O_4 end-member (sample MgV100) resulted in spinel crystals with a substantial component of the inverse spinel $V^{4+}Mg_2O_4$ (Rudorff and Reuter 1947). The reason why we obtained a significant component (ca. 26%) of $V^{4+}Mg_2O_4$ in this particular sample may be related to the synthesis conditions in terms of melt composition. The MgV100 run was performed without the $Na_2B_4O_7$ flux compound, because the large amount of V_2O_5 in this case acts like a flux in itself (melting point of 690 °C), and adding also $Na_2B_4O_7$ would decrease saturation levels and hence inhibit nucleation and crystallization. The only components in this run is MgO and V_2O_5, and when the melt during the cooling phase becomes saturated with MgO, the increasing activity of MgO will stabilize the formation of Mg-rich phases. The $V^{4+}Mg_2O_4$ phase can hence be expected to be stabilized compared to the less Mg-rich MgV_2O_4 phase. Since all the other runs contained also $Na_2B_4O_7$ and Al_2O_3, both MgO and V_2O_5 were more diluted in these melts. The Al-bearing spinels do show a slight solid solution with $V^{4+}Mg_2O_4$, but with amounts very close to the analytical error (Table 2).

Consequently, our samples are best described in the three-component system $MgAl_2O_4$-MgV_2O_4-VMg_2O_4. In order to attain a complete picture of the structural relations, we included crystal chemical data from the literature for the end-members of this system, which show the following structural formulae: $^{T}(Mg_{0.76}Al_{0.24})^{M}(Mg_{0.24}Al_{1.76})O_4$, $^{T}(Mg)^{M}(V^{3+})_2O_4$ and $^{T}(Mg)^{M}(MgV^{4+})O_4$ (Rudorff and Reuter 1947; Mamiya and Onoda 1995; Andreozzi et al. 2001). Data for Al-free magnesium vanadate spinels $^{T}(Mg)^{M}(Mg_{0.316}V^{3+}_{1.368}V^{4+}_{0.316})O_4$, $^{T}(Mg_{0.974})^{M}(V^{3+}_{1.596}V^{4+}_{0.316})O_4$ and $^{T}(Mg_{0.969}Fe^{3+}_{0.031})^{M}(Mg_{0.632}V^{3+}_{0.766}V^{4+}_{0.602})O_4$ were also included in this study (Righter et al 2006; Uchida et al. 2007). On this basis, the crystal chemistry of V^{3+}- and V^{4+}-bearing spinels can be assessed along the two series $MgAl_2O_4$-MgV_2O_4 and MgV_2O_4-VMg_2O_4.

Series $MgAl_2O_4$-MgV_2O_4

Vanadium-bearing spinels of this series can be represented by the general structural formula $^{T}(Mg_{1-i}Al_i)^{M}(Mg_iAl_{2-i-2x}V^{3+}_{2x})O_4$ where x represents the substitution $V^{3+} \rightarrow Al$ at the M site and i is the Mg-Al disorder over T and M (also known as cation inversion). In the analyzed samples, the inversion parameter i decreases from 0.23 to 0.00 with increasing V^{3+} content (Table 3). Therefore, this normal spinel series shows a moderately disordered cation distribution for the Al-rich compositions (e.g., crystals MgV20c and MgV60b) which becomes fully ordered for the V-rich compositions (crystals MgV90c32 and MgV90c33).

All analyzed samples are chemically quite homogenous as shown by the standard deviations of the weight percent oxides (Table 3), except crystal MgV80aC. Although this sample is a single crystal from an X-ray diffraction viewpoint, EMP spot analyses indicate compositional variations in Al (0.70-1.18 apfu) and V (0.79-1.29 apfu), whereas Mg is practically constant (ca. 1.01 apfu). SEM/EDS X-ray mapping of a crystal fragment from sample MgV80aC displays the chemical zonation of V against Al (Fig. 1). In detail, a V enrichment (and Al depletion) is observed in the core region of the crystal. This zoned sample represents the transition spinel *sensu stricto*-magnesiocoulsonite and confirms the occurrence of a complete solid solution along the series $MgAl_2O_4$-MgV_2O_4.

Recorded optical absorption spectra (Fig. 2) show two intense and broad bands at ~23900 and ~18200 cm^{-1} (418 and 549 nm), marking the spin-allowed electronic $^3T_{1g} \rightarrow {}^3T_{2g}$ (^3F) and $^3T_{1g} \rightarrow {}^3T_{1g}$ (^3P) transitions in octahedrally coordinated V^{3+} (e.g., Burns 1993 and references therein). The absence of absorption bands in the spectral range below 15000 cm^{-1} demonstrates that the measured spinels contain no, or negligible contents of, V^{4+} (e.g., Kato et al. 1974) or of tetrahedrally coordinated V^{3+} (e.g., Kück and Jander 1999).

Series MgV_2O_4-VMg_2O_4

Vanadium-bearing spinels of this series can be represented by the general structural formula $^{T}(Mg)^{M}(Mg_xV^{3+}_{2-2x}V^{4+}_x)O_4$ where x represents the substitution $(V^{4+} + Mg) \rightarrow 2V^{3+}$. Due to the accommodation of $(V^{4+} + Mg)$ at the M site the cation distribution changes from that typical of the normal 2-3 spinel, $^{T}(Mg)^{M}(V)_2O_4$, to that of the inverse 4-2 spinel $^{T}(Mg)^{M}(MgV)O_4$.

Crystal chemistry

Two different types of substitutions relate the MgV_2O_4 to $MgAl_2O_4$ and to VMg_2O_4: $V^{3+} \leftrightarrow Al$ and $2V^{3+} \leftrightarrow V^{4+} + Mg$, respectively.

Figure 3 shows that the unit-cell parameter clearly increases from 8.085 Å to 8.432 Å with increasing V^{3+} along the series $MgAl_2O_4$-MgV_2O_4, but only slightly increases from 8.386 Å to 8.432 Å with increasing V^{3+} along the series VMg_2O_4-MgV_2O_4. This is consistent with the larger difference between the $^{VI}V^{3+}$ and $^{VI}Al^{3+}$ ionic radii (0.66 Å and 0.55 Å, respectively) compared to that between $^{VI}V^{3+}$ and the aggregate constituent $^{VI}(Mg^{2+}V^{4+})$, the latter with a cation radius of 0.65 Å (calculated from Shannon 1976). As the main substitutions occur at the M site, the M-O bond distance practically mimics the trend of the unit-cell parameter.

The tetrahedral bond distance, which depends on the substitution $^{T}Al \rightarrow {}^{T}Mg$, increases with increasing Mg content (Fig. 4) due to the difference in the ^{IV}Mg and ^{IV}Al ionic radii (0.57 Å and 0.39 Å, respectively), as well as the "dragging effect" of V^{3+} on the ^{T}Mg-O distance (i.e., variation in concentration of $^{M}V^{3+}$ may cause variations in T-O distance), which is responsible for the increase of ^{T}Mg-O from 1.966 Å (typical of spinel *sensu stricto*) to 1.971 Å, as observed by Lavina et al. (2003) and Uchida et al. (2007) in a suite of vanadian magnesiochromite crystals from the Sludyanka metamorphic complex, and a synthetic magnesium vanadate spinel (respectively). This lengthening of ^{T}Mg-O seems to extend to the end-member $^{T}(Mg)^{M}(MgV)O_4$, which has ^{T}Mg-O = 1.975 (Rudorff and Reuter 1947).

In addition to previous studies of the $MgAl_2O_4$-MgV_2O_4-VMg_2O_4 system, the results presented here demonstrate that complete solid solution occur between $MgAl_2O_4$ and MgV_2O_4 as well as between MgV_2O_4 and VMg_2O_4, and that the cation size mismatch associated with the respective substitutions can be accommodated by the spinel structure. It could be expected that solid solution would also occur between the $MgAl_2O_4$ and VMg_2O_4 end members. However, this seems not to be the case, as no samples containing relevant amounts of V^{4+}, V^{3+} and Al in solid solution to our knowledge have been reported, and our attempts to synthesize samples along this join were unsuccessful. We looked for crystal-chemical reasons for which the cation arrangements V^{3+}-Al seem to be more compatible in the spinel crystal structure than arrangements V^{4+}-Al, but could not find any specific arguments from bond-valence considerations (i.e., no relevant strain in the bonds) nor cation size mismatch (size differences among V^{4+}, V^{3+} and Al are consistent with the occurrence of extensive solid solutions). In addition, we observe that the amounts of V^{4+} are nearly

insignificant in all synthetic Al-bearing vanadate spinels, even in the magnesiocoulsonite crystals MgV90c32 and MgV90c33, which contain only 0.06 apfu of Al. By contrast, in the Al-free vanadate spinel (sample MgV100), the amounts of V^{4+} increase to a significant value of 0.26 apfu (Table 2). Since all the studied samples were synthetized under the same experimental conditions of temperature and oxygen fugacity (close to the NNO buffer), the presence or the absence of V^{4+} seems to be a result of bulk/melt chemical composition from which the spinels were formed (e.g., presence or absence of Al_2O_3 and $Na_2B_4O_7$).

IMPLICATIONS

The accommodation of transition metals in the spinel structure is a function of intensive variables such as temperature, oxygen fugacity and composition; and spinel stability is the main factor that controls the distribution of V in basaltic rocks (e.g., Righter et al. 2006a and references therein). Results from experiments carried out under similar temperature and oxygen fugacity conditions demonstrate that differences in V valence in Cr-bearing spinel and magnetite may be attributed to crystal chemical effects (in terms of the normal *versus* inverse spinel structures): the inverse spinel magnetite favors V^{4+} more than normal-spinel chromite showing that the position of equilibrium redox boundary may change in accordance with the normal or inverse cation distribution of spinel (Righter et al. 2006a,b). An interesting observation of the present study is that despite the observed full solid-solution along the $MgAl_2O_4$-MgV_2O_4 and MgV_2O_4-VMg_2O_4 series, the spinel structure seems to be unable to stabilize V^{4+} in any intermediate members on the $MgAl_2O_4$-Mg_2VO_4 join even at high oxygen fugacities as those prevailing under ambient atmosphere conditions. This behavior contrasts to results on spinels synthesized under comparable or even lower oxygen fugacities in systems containing additional elements as, e.g., Fe, Cr and Ti (Righter et al. 2006a,b), and indicates that the accommodation of specific V-valences can be strongly influenced by crystal-structural constraints. This further implies that any evaluation of oxygen fugacities during mineral formation based exclusively on V cation valence distributions in spinel should be treated with caution. The results of our present study underline that the V cation valency distribution in spinels is not exclusively reflecting oxygen fugacities, but also depends on activities and solubilities of all chemical components in the crystallization environment.

ACKNOWLEDGEMENTS

The authors appreciate constructive reviews by Thomas Armbruster and an anonymous reviewer, and the manuscript handling by the Associate Editor Kristina Lilova. Chemical analyses were carried out with the kind assistance of M. Serracino to whom the authors express their gratitude. F.B. is grateful to financial support from the project Università Sapienza 2014. R.A.F. is grateful to the Swedish Museum of Natural History that partly funded her visit at Stockholm laboratories for this project.

REFERENCES CITED

Andreozzi, G.B., Bosi, F. and Garramone, F. (2001) Synthetic spinels in the $(Mg,Fe^{2+},Zn)(Al,Fe^{3+})_2O_4$ system. II. Preliminary chemical and structural data of hercynite and magnesioferrite samples. Periodico di Mineralogia, 70, 193–204.

Bosi, F., Hålenius, U., and Skogby, H. (2010) Crystal chemistry of the $MgAl_2O_4$-$MgMn_2O_4$-$MnMn_2O_4$ system: Analysis of structural distortion in spinel- and hausmannite-type structures. American Mineralogist, 95, 602–607.

Burns R.G. (1993) Mineralogical Applications of Crystal Field Theory, pp. 551. 2nd edition. Cambridge University Press, Cambridge.

Canil, D. (1999) Vanadium partitioning between orthopyroxene, spinel, and silicate melt and the redox states of mantle source regions for primary magmas. Geochimica et Cosmochimica Acta, 63, 557–572.

Carbonin, S., Russo, U., and Della Giusta, A. (1996) Cation distribution in some natural spinels from X−ray diffraction and Mössbauer spectroscopy. Mineralogical Magazine, 60, 355–368.

Connolly, H.C., Jr. and Burnett, D.S. (2003) On Type B CAI formation: Experimental constraints on f_{O2} variations in spinel minor element partitioning and reequilibration effects. Geochimica et Cosmochimica Acta, 67, 4429–4434.

Della Giusta, A., Princivalle, F., and Carbonin, S. (1986) Crystal chemistry of a suite of natural Cr-bearing spinels with $0.15 \leq Cr \leq 1.07$. Neues Jahrbuch für Mineralogie Abhandlungen, 155, 319–330.

Huebner, J.S. and Sato, M. (1970) The oxygen fugacity-temperature relationships of manganese oxide and nickel oxide buffers. American Mineralogist, 55, 934-952.

Kato, K., Sugitani, Y., and Nagashima, K. (1974) Absorption spectrum of barium vandyl silicate $BaVOSi_2O_6$. Mineralogical Journal, 7, 421–430.

Kück, S. and Jander, P. (1999) Luminescence from V^{3+} in tetrahedral oxo-coordination. Chemical Physics Letters, 300, 189–194.

Lavina, B., Salviulo, G., and Della Giusta, A. (2002) Cation distribution and structure modeling of spinel solid solutions. Physics and Chemistry of Minerals, 29, 10–18.

Lavina, B., Reznitskii, L.Z., and Bosi, F. (2003) Crystal chemistry of some Mg, Cr, V normal spinels from Sludyanka (Lake Baikal, Russia): the influence of V^{3+} on structural stability. Physics and Chemistry of Minerals, 30, 599–605.

Liu, R.S., Cheng, Y.C., Gundakaram, R., and Jang, L.Y. (2001) Crystal and electronic structures of inverse spinel-type $LiNiVO_4$. Materials Research Bulletin, 36, 1479–1486.

Mamiya, H. and Onoda, M. (1995) Electronic states of vanadium spinels MgV_2O_4 and ZnV_2O_4. Solid State Communications, 95, 217–221.

Papike, J.J., Karner, J.M., and Shearer, C.K. (2005) Comparative planetary mineralogy: valence state partitioning of Cr, Fe, Ti, and V among crystallographic sites in olivine, pyroxene, and spinel from planetary basalts. American Mineralogist, 90, 277–290.

Pouchou, J.L. and Pichoir, F. (1984) A new model for quantitative X-ray micro-analysis. I. Application to the analysis of homogeneous samples. La Recherche Aérospatiale, 3, 13–36.

Radtke, A. S. (1962) Coulsonite, FeV_2O_4, a spinel-type mineral from Lovelock, Nevada. American Mineralogist, 47, 1284–1291.

Righter, K., Sutton, S.R., Newville, M., Le, L., Schwandt, C.S., Uchida, H., Lavina, B., and Downs, R.T. (2006a) An experimental study of the oxidation state of vanadium in spinel and basaltic melt with implication for the origin of planetary basalt. American Mineralogist 91, 1643–1656.

Righter, K., Leeman, W.P., and Hervig, R.L. (2006b) Partitioning of Ni, Co, and V between spinel-structured oxides and silicate melts: Importance of spinel composition. Chemical Geology, 227, 1–25.

Reznitskii, L.Z., Sklyarov, E.V., and Ushchapovskaya, Z.F. (1995) Magnesiocoulsonite MgV_2O_4—A new mineral species in the spinel group. Zapiski Rossiiskogo Mineralogicheskogo Obshchestva, 124, 91–98 (in Russian).

Rudorff, W. and Reuter, B. (1947) Die Struktur der Magnesium- und Zink-Vanadinspinelle. Zeitschrift fur Anorganische und Allgemeine Chemie, 253, 194–208.

Shannon, R.D. (1976) Revised effective ionic radii and systematic studies of interatomic distances in halides and chalcogenides. Acta Crystallographica, A, 32, 751–767.

Sheldrick, G.M. (2013) SHELXL2013. University of Göttingen, Germany.

Sutton, S.R., Karner, J., Papike, J.J., Delaney, J.S., Shearer, C.K., Newville, M., Eng, P., Rivers, M., and Dyar, M.D. (2005) Vanadium K-edge XANES of synthetic and natural basaltic glasses and applications to microscale oxygen barometry. Geochimica et Cosmochimica Acta, 69, 2333–2348.

Uchida, H. Righter, K. Lavina, B. Nowell, M.M., Wright, S.I., Downs, R.T., and Yang, H. (2007) Investigation of synthetic $Mg_{1.3}V_{1.7}O_4$ spinel with MgO inclusions: Case study of a spinel with an apparently occupied interstitial site. American Mineralogist, 92, 1031–1037.

Zakrzewski, M.A., Burke, E.A.J., and Lustenhouwer, W.J. (1982) Vuorelainenite, a new spinel, and associated minerals from the Sätra (Doverstorp) pyrite deposit, central Sweden. Canadian Mineralogist, 20, 281–290.

LIST OF TABLES

LIST OF FIGURES AND FIGURE CAPTIONS

TABLE 1. Experimental conditions and products of the crystal synthesis runs under reducing conditions

Synthesis Run	MgV20c	MgV40a	MgV60b	MgV80a	MgV90c	MgV100a
			Experimental Conditions			
Nutrients weight fraction:						
MgO	0.29	0.27	0.25	0.23	0.22	0.22
V_2O_5	0.26	0.39	0.54	0.67	0.73	0.78
Al_2O_3	0.44	0.33	0.20	0.09	0.05	0.00
Total	1.00	1.00	1.00	1.00	1.00	1.00
Flux/nutrients ratio	1.00	0.80	0.60	0.30	0.15	0.00
$\log(P_{CO_2}/P_{H_2})$	1.6	1.6	1.6	1.6	1.6	1.6
			Synthesis Products			
Product Minerals	sp, Mg-brt	sp, Mg-brt	sp, Mg-brt	sp, V-ox, Mg-brt	sp, V-ox, Mg-brt	sp, V-ox
Spinel crystals:						
max. dimensions	200 μm	220 μm	210 μm	800 μm	1 mm	1 mm
color	reddish-orange	deep reddish to reddish-brown	deep reddish to brownish-black	zoned brownish-black	zoned brownish-black	black

Notes : All synthesis experiments were performed by slow cooling from 1200 to 800 °C. The fixed CO_2 to H_2 ratio imposes a variation in oxygen fugacity from approximately 10^{-8} to 10^{-15} bars. sp = spinel; Mg-brt = Mg-borates (warwickite); V-ox = Vanadium oxides (karelianite: V_2O_3).

TABLE 2. Selected X-ray diffraction data for the analyzed spinels in $(Mg,Al,V)_3O_4$

Crystal	MgV20c	MgV60b	MgV80aN	MgV90c27	MgV80aC	MgV90c33	MgV90c32	MgV100a
Crystal sizes (mm)	0.20×0.20×0.18	0.32×0.27×0.25	0.34×0.30×0.20	0.20×0.20×0.16	0.21×0.20×0.19	0.40×0.38×0.12	0.20×0.18×0.14	0.26×0.26×0.12
a (Å)	8.1227(2)	8.1358(3)	8.1710(4)	8.1723(2)	8.2682(3)	8.4048(2)	8.4031(3)	8.4100(3)
u	0.26193(3)	0.26184(4)	0.26178(3)	0.26175(3)	0.26118(4)	0.26021(5)	0.26025(5)	0.26034(6)
T-O (Å)	1.9265(5)	1.9283(5)	1.9358(5)	1.9357(4)	1.9503(6)	1.9683(8)	1.9684(8)	1.9715(9)
M-O (Å)	1.9386(2)	1.9424(3)	1.9513(3)	1.9518(2)	1.9789(3)	2.0190(4)	2.0184(4)	2.0192(5)
T-m.a.n.	12.3(1)	12.2(1)	12.2(1)	12.5(1)	12.2(1)	12.0	12.0	12.0
M-m.a.n.	13.6(1)	14.2(1)	15.3(1)	15.5(1)	18.0(1)	22.3(1)	22.1(1)	21.3(1)
T-U^{11} (Å^2)	0.00468(10)	0.00558(12)	0.00593(10)	0.00589(9)	0.00662(12)	0.00507(8)	0.00566(14)	0.00610(16)
M-U^{11} (Å^2)	0.00448(8)	0.00517(10)	0.00547(7)	0.00543(6)	0.00557(6)	0.00507(8)	0.00502(7)	0.00590(10)
M-U^{12} (Å^2)	-0.00019(3)	-0.00023(4)	-0.00022(3)	-0.00022(3)	-0.00022(3)	-0.00022(2)	-0.00020(3)	-0.00024(2)
O-U^{11} (Å^2)	0.00806(9)	0.00894(13)	0.00921(9)	0.00920(8)	0.00934(11)	0.00663(14)	0.00668(13)	0.00818(16)
O-U^{12} (Å^2)	-0.00004(7)	-0.00019(8)	-0.00040(7)	-0.00043(6)	-0.00049(8)	-0.00036(9)	-0.00043(9)	-0.00075(9)
Reciprocal space range *hkl*	$-16 \le h \le 14$	$-14 \le h \le 13$	$-12 \le h \le 16$	$-16 \le h \le 13$	$-16 \le h \le 13$	$-12 \le h \le 16$	$-12 \le h \le 16$	$-13 \le h \le 16$
	$-15 \le k \le 15$	$-14 \le k \le 14$	$-11 \le k \le 16$	$-16 \le k \le 13$	$-13 \le k \le 15$	$-14 \le k \le 16$	$-13 \le k \le 16$	$-13 \le k \le 16$
	$-10 \le l \le 16$	$-16 \le l \le 12$	$-16 \le l \le 12$	$-16 \le l \le 13$	$-15 \le l \le 16$	$-16 \le l \le 14$	$-16 \le l \le 13$	$-16 \le l \le 11$
EXTI	0.0042(4)	0.0036(12)	0.0044(10)	0.0009(3)	0.0009(4)	0.0046(7)	0.0057(5)	0.035(2)
Set of read reflections	2485	2408	2463	2549	2533	2715	2755	2735
Unique reflections	132	133	136	136	141	146	147	148
R int. (%)	0.94	0.81	0.70	0.71	0.52	1.14	0.84	1.46
*R*1 (%) all reflections	1.00	1.01	0.88	0.85	0.86	1.09	1.09	1.46
*wR*2 (%) all reflections	2.24	2.50	2.21	2.11	2.43	3.23	3.01	3.89
GooF	1.179	1.296	1.272	1.143	1.261	1.230	1.302	1.394
Diff. Peaks (±*e*/Å^3)	–0.19; 0.21	–0.26; 0.19	-0.18; 0.19	-0.17; 0.22	-0.17; 0.29	-0.35; 0.42	-0.28; 0.38	-0.40; 0.73

Notes: *a* = unit-cell parameter; *u* = oxygen fractional coordinate; T-O and M-O = tetrahedral and octahedral bond lengths, respectively; T- and M-m.a.n.. = T- and M-mean atomic number; U^{11} = atomic displacement parameter; $U^{11} = U^{22} = U^{33}$ and $U^{12} = U^{13} = U^{23}$ (= 0 for *T*-site due to symmetry reasons); EXTI = extinction parameter; *R* int. = merging residual value; *R*1 = discrepancy index, calculated from *F*-data; *wR*2 = weighted discrepancy index, calculated from F^2-data; GooF = goodness of fit; Diff. Peaks = maximum and minimum residual electron density. Radiation, Mo-$K\alpha$ = 0.71073 Å. Data collection temperature = 293 K. Total number of frames = 1500. Range for data collection 8° < 2θ < 91°. Origin fixed at $\bar{3}m$. Space group $Fd\bar{3}m$. *Z* = 8. Spinel structure has cations at Wyckoff positions 8*a* ≡ T (1/8, 1/8, 1/8) and 16*d* ≡ M (1/2, 1/2, 1/2), and oxygen anions at 32*e* (*u*, *u*, *u*).

TABLE 3. Chemical composition of the synthetic spinels $(Mg,Al,V)_3O_4$

Sample	MgV20c	MgV60b	MgV80aN	MgV90c27	MgV80aC	MgV90c33	MgV90c32	MgV100a
$V_2O_{3\ total}$ (wt%)	8.99(41)	13.46(79)	22.99(1.46)	24.71(1.21)	44.86(6.97)	75.20(32)	76.02(30)	70.95(30)
Al_2O_3	63.03(45)	58.95(42)	50.80(1.49)	48.04(1.79)	30.61(6.53)	1.72(11)	1.51(11)	-
MgO	27.42(15)	27.17(27)	26.71(10)	26.93(18)	24.68(75)	22.24(21)	22.50(44)	27.59(17)
V_2O_3*	8.88	13.15	22.44	23.11	44.23	73.54	74.21	60.41
VO_2*	0.13	0.34	0.61	1.78	0.70	1.83	2.00	11.67
Total	99.46	99.61	100.55	99.86	100.25	99.34	100.22	99.67
V^{4+} (apfu)	0.002	0.006	0.011	0.033	0.014	0.042	0.045	0.259
V^{3+}	0.174	0.262	0.457	0.477	0.977	1.853	1.854	1.482
Al	1.821	1.726	1.521	1.457	0.995	0.064	0.056	-
Mg	1.002	1.006	1.011	1.033	1.014	1.042	1.045	1.259
Total	3.000	3.000	3.000	3.000	3.000	3.000	3.000	3.000
			End member					
$MgAl_2O_4$ (%)	91	87	76	74	50	3	3	0
$MgV^{3+}{}_2O_4$	9	13	23	24	49	95	95	85
$Mg_2V^{4+}O_4$	-	-	1	2	1	2	2	15

Notes : Cations on the basis of 4 oxygen atoms per formula unit (apfu).
* Determined from stoichiometry.

Table 4. Empirical structural formula of the analyzed spinels $(Mg,Al,V)_3O_4$

Sample	Structural formula
MgV20c	$^{T}(Mg_{0.77}Al_{0.23})\ ^{M}(Mg_{0.23}Al_{1.59}V^{3+}_{0.17})O_4$
MgV60b	$^{T}(Mg_{0.78}Al_{0.22})\ ^{M}(Mg_{0.22}Al_{1.51}V^{3+}_{0.26}V^{4+}_{0.01})O_4$
MgV80aN	$^{T}(Mg_{0.82}Al_{0.18})\ ^{M}(Mg_{0.19}Al_{1.34}V^{3+}_{0.46}V^{4+}_{0.01})O_4$
MgV90c27	$^{T}(Mg_{0.82}Al_{0.18})\ ^{M}(Mg_{0.21}Al_{1.28}V^{3+}_{0.48}V^{4+}_{0.03})O_4$
MgV80aC	$^{T}(Mg_{0.89}Al_{0.11})\ ^{M}(Mg_{0.12}Al_{0.89}V^{3+}_{0.98}V^{4+}_{0.01})O_4$
MgV90c33	$^{T}(Mg_{1.00})\ ^{M}(Mg_{0.04}Al_{0.06}V^{3+}_{1.85}V^{4+}_{0.04})O_4$
MgV90c32	$^{T}(Mg_{1.00})\ ^{M}(Mg_{0.05}Al_{0.06}V^{3+}_{1.85}V^{4+}_{0.05})O_4$
MgV100a	$^{T}(Mg_{1.00})\ ^{M}(Mg_{0.26}V^{3+}_{1.48}V^{4+}_{0.26})O_4$

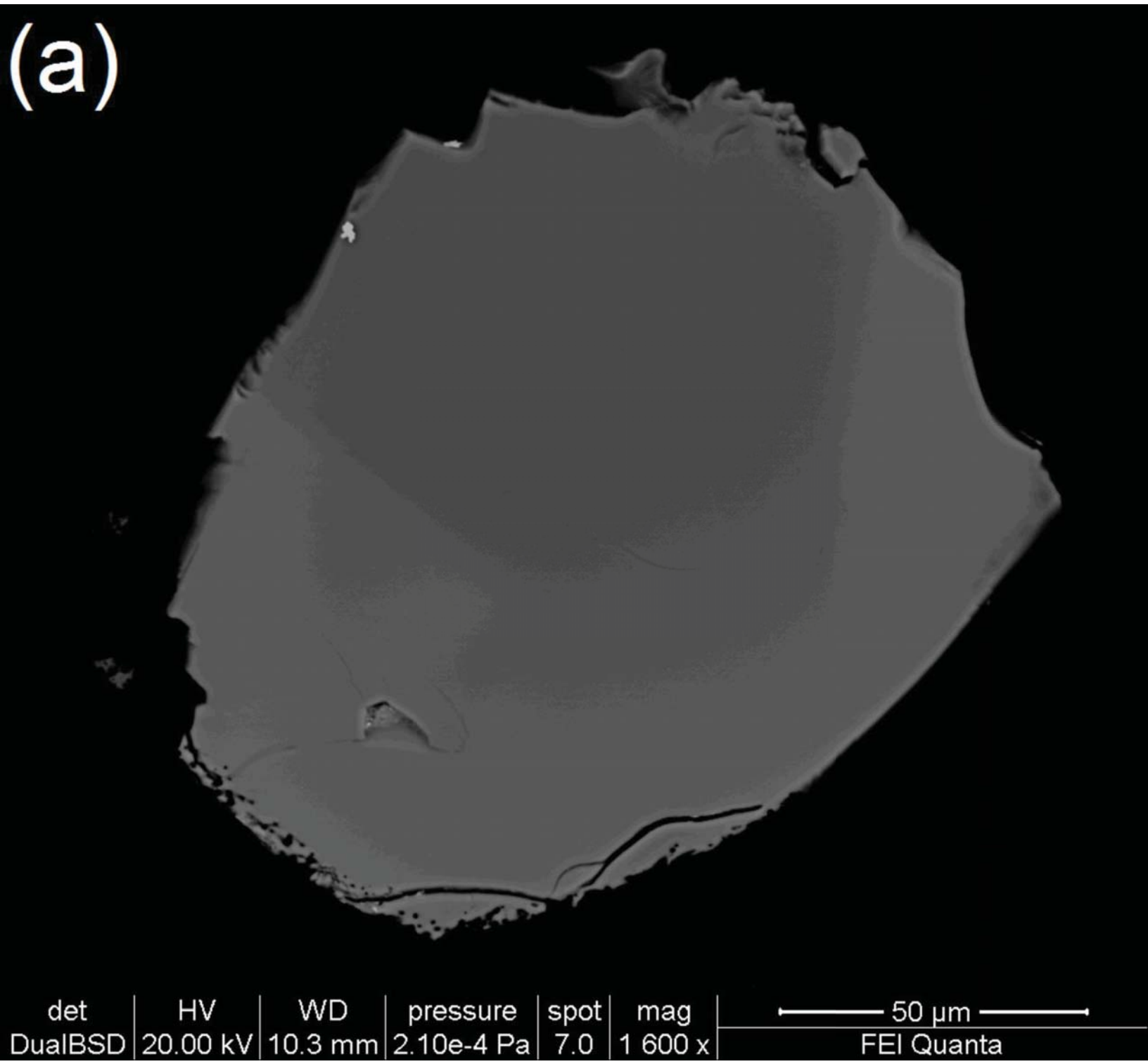
(a)
det
DualBSD
HV
20.00 kV
WD
10.3 mm
pressure
2.10e-4 Pa
spot
7.0
mag
1 600 x
50 µm
FEI Quanta

This is a preprint, the final version is subject to change, of the American Mineralogist (MSA)
Cite as Authors (Year) Title. American Mineralogist, in press.
(DOI will not work until issue is live.) DOI: http://dx.doi.org/10.2138/am-2016-5508

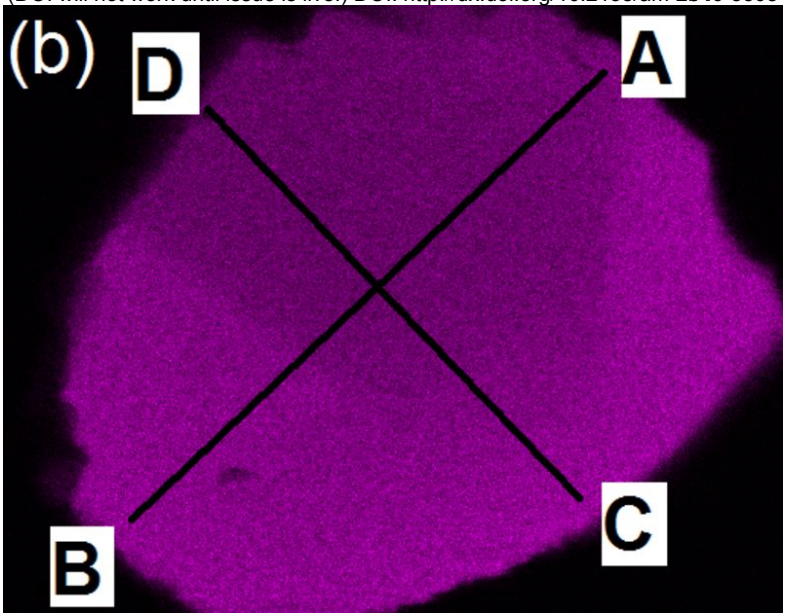

This is a preprint, the final version is subject to change, of the American Mineralogist (MSA)
Cite as Authors (Year) Title. American Mineralogist, in press.
(DOI will not work until issue is live.) DOI: http://dx.doi.org/10.2138/am-2016-550811/4

Figure 1(c)

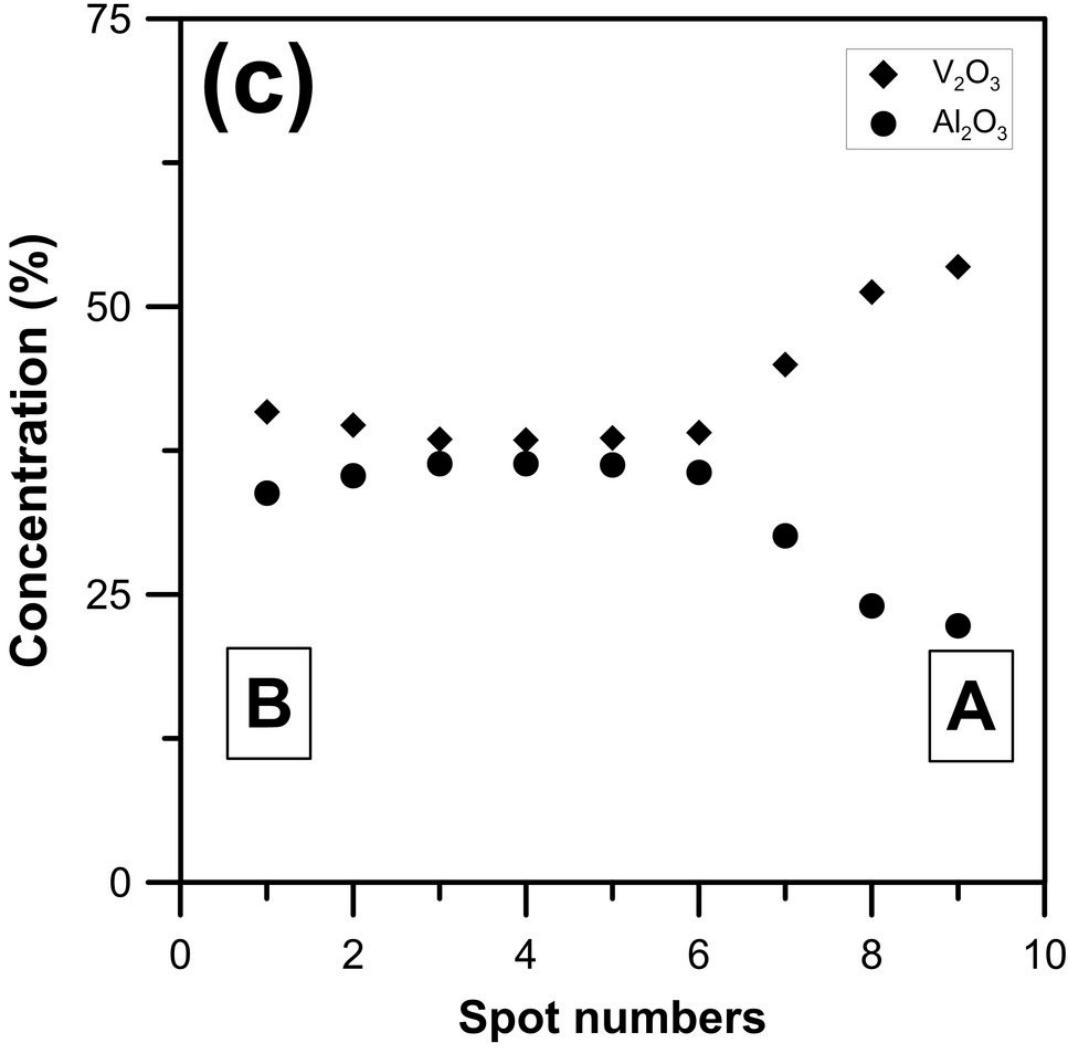

This is a preprint, the final version is subject to change, of the American Mineralogist (MSA)
Cite as Authors (Year) Title. American Mineralogist, in press.
(DOI will not work until issue is live.) DOI: http://dx.doi.org/10.2138/am-2016-550811/4

Figure 1(d)

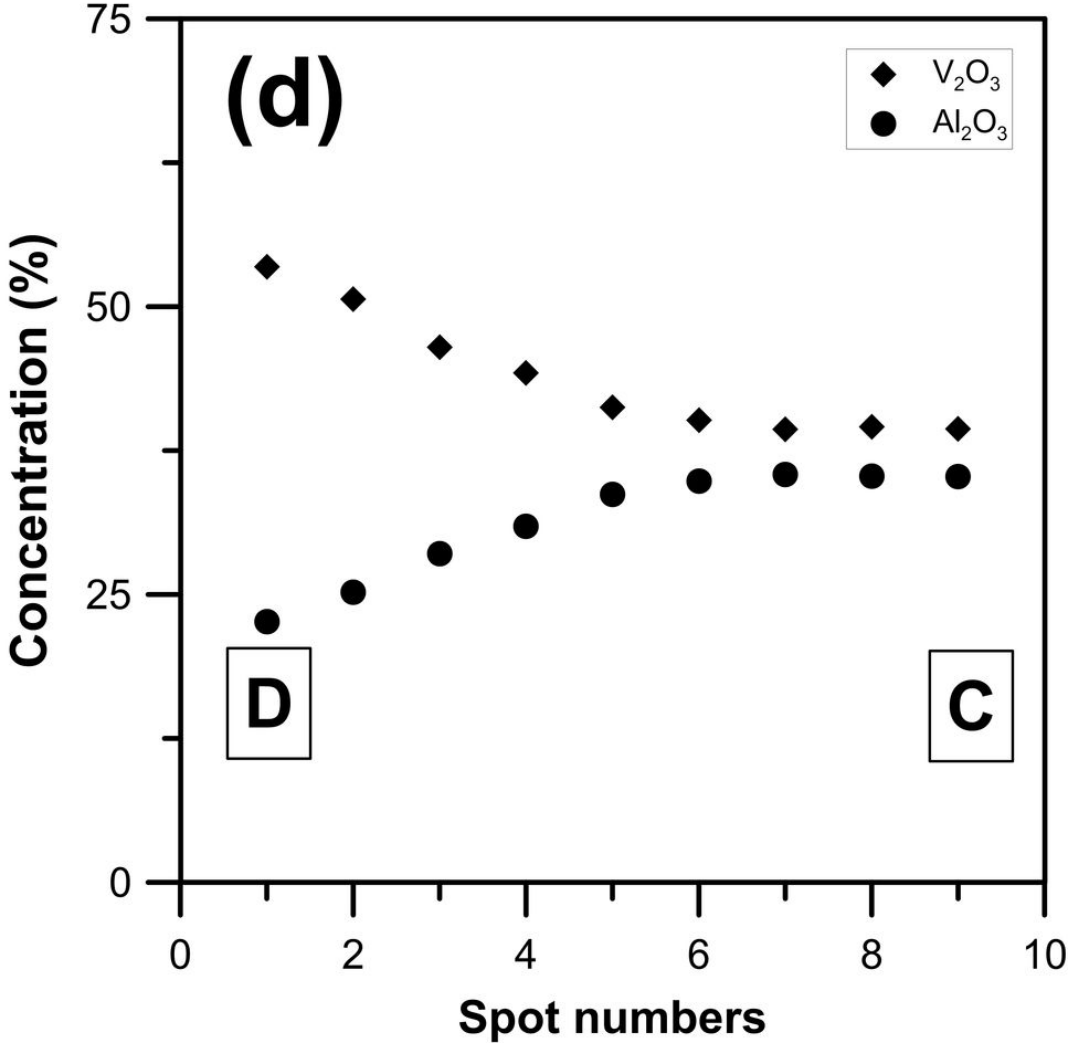

Fig. 2

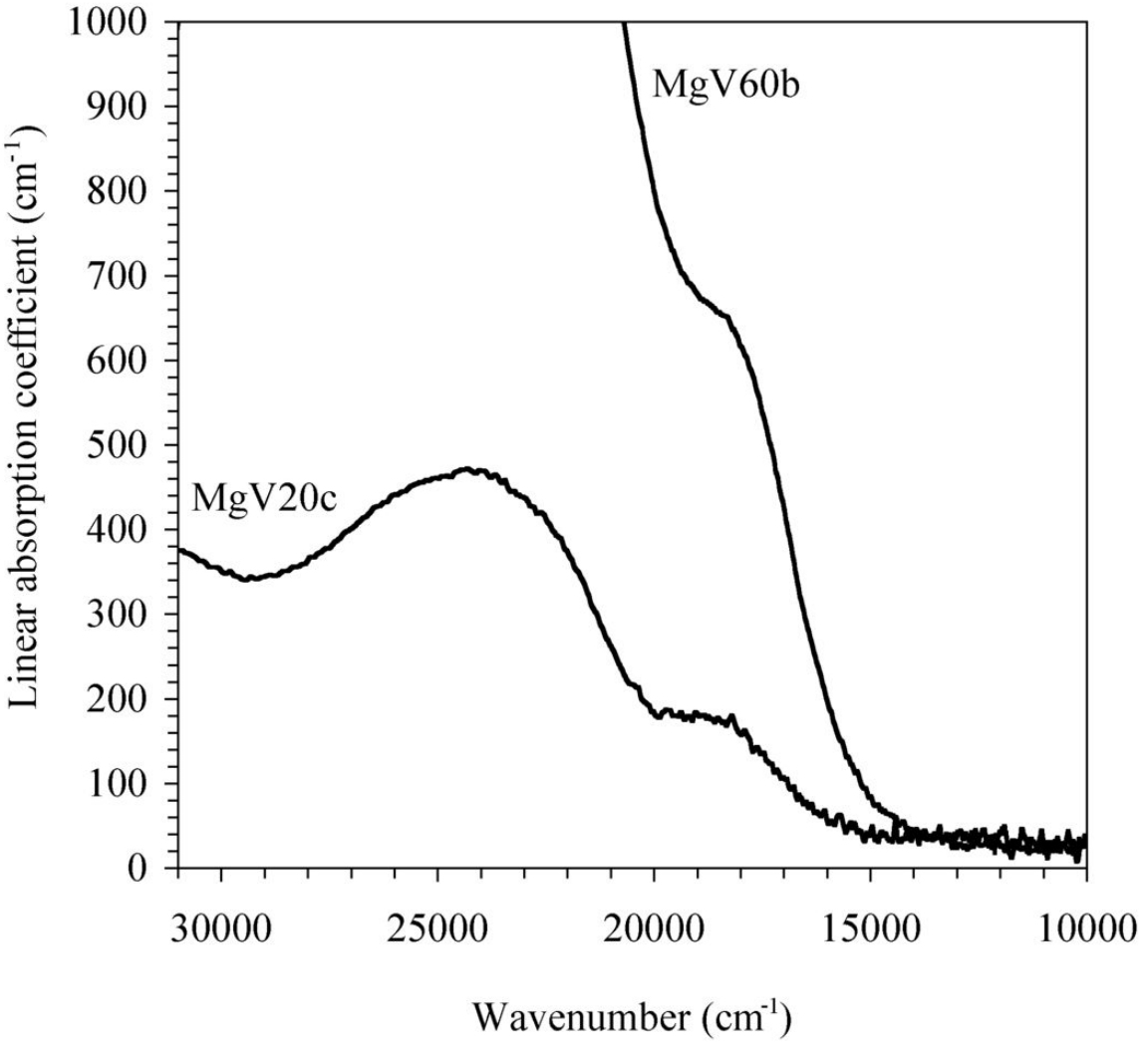
MgV60b
MgV20c
Linear absorption coefficient (cm-1)
Wavenumber (cm-1)
1000
900
800
700
600
500
400
300
200
100
0
30000
25000
20000
15000
10000

Figure 3

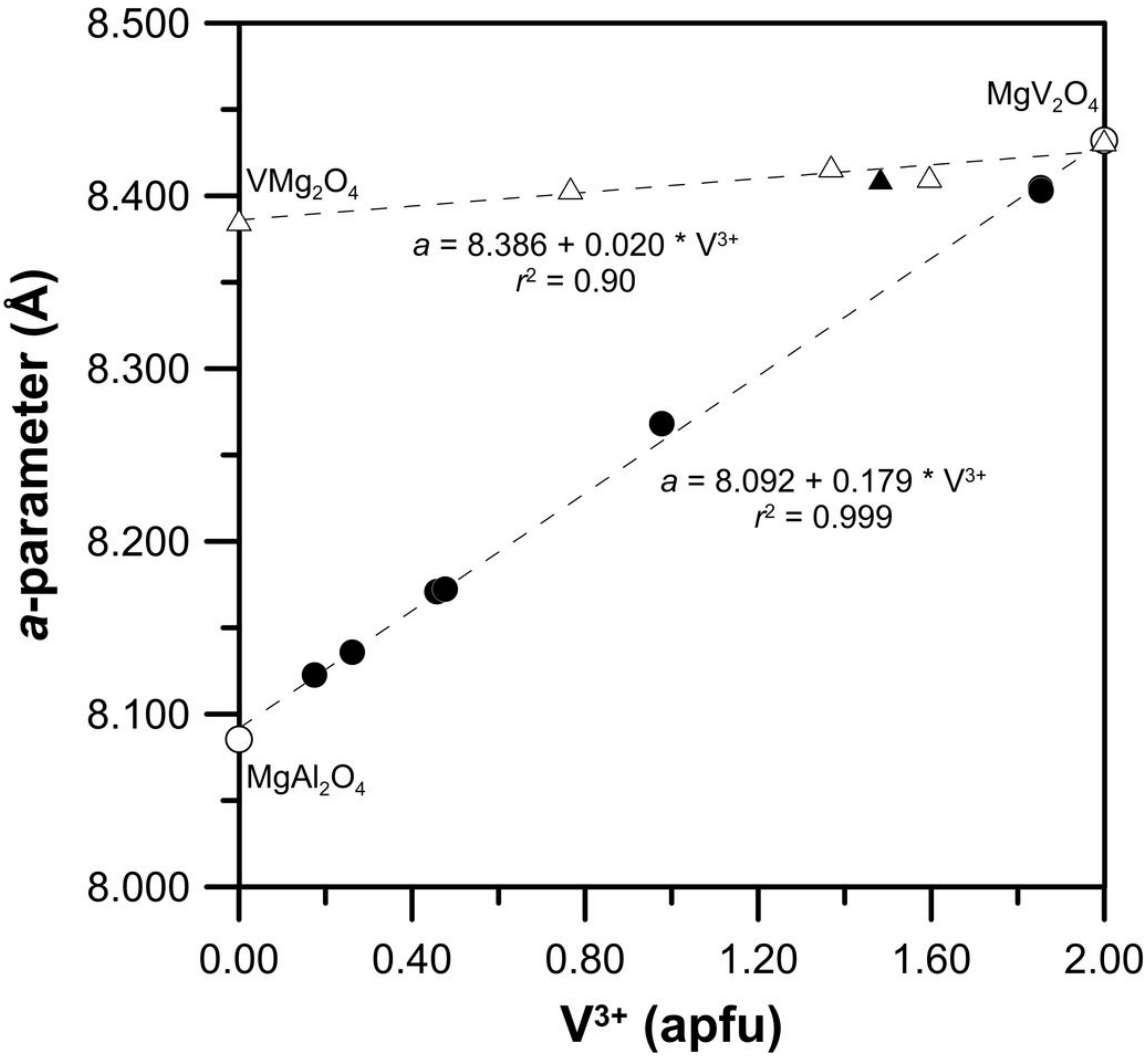
8.500
8.400
8.300
8.200
8.100
8.000
a-parameter (Å)
0.00
0.40
0.80
1.20
1.60
2.00
V3+ (apfu)
MgV2O4
VMg2O4
MgAl2O4
a = 8.386 + 0.020 * V3+
r2 = 0.90
a = 8.092 + 0.179 * V3+
r2 = 0.999

Figure 4

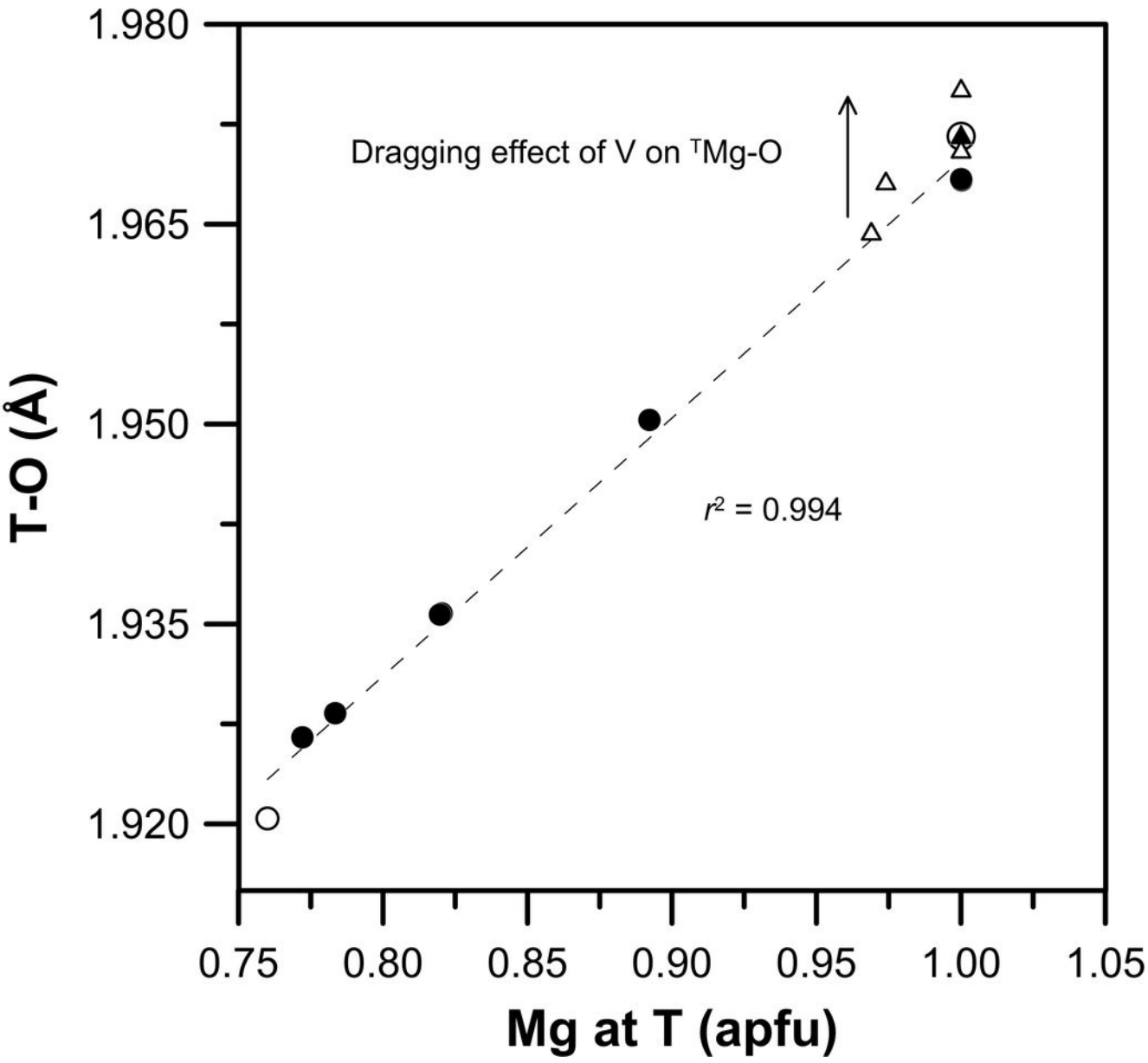
Dragging effect of V on TMg-O
r2 = 0.994
T-O (Å)
1.980
1.965
1.950
1.935
1.920
0.75
0.80
0.85
0.90
0.95
1.00
1.05
Mg at T (apfu)